Asociación Argentina
de Mecánica Computacional

Mecánica Computacional Vol XXVI, pp.1747-1773
Sergio A. Elaskar, Elvio A. Pilotta, Germán A. Torres (Eds.)
Córdoba, Argentina, Octubre 2007

A NUMERICAL PROCEDURE TO ESTIMATE THE EFFECTIVE MODULI IN HIGHLY HETEROGENEOUS FLUID-SATURATED POROUS MEDIA

J. Germán Rubino[a], Claudia L. Ravazzoli[b] and Juan E. Santos[c]

[a]*CONICET, Departamento de Geofísica Aplicada, Facultad de Ciencias Astronómicas y Geofísicas, Universidad Nacional de La Plata, Paseo del Bosque S/N, La Plata (1900) Argentina, grubino@fcaglp.fcaglp.unlp.edu.ar ,*
[b]*CONICET, Departamento de Geofísica Aplicada, Facultad de Ciencias Astronómicas y Geofísicas, Universidad Nacional de La Plata, Paseo del Bosque S/N, La Plata (1900) Argentina, claudia@fcaglp.fcaglp.unlp.edu.ar,*
[c]*CONICET, Departamento de Geofísica Aplicada, Facultad de Ciencias Astronómicas y Geofísicas, Universidad Nacional de La Plata, Paseo del Bosque S/N, La Plata (1900) Argentina, santos@fcaglp.fcaglp.unlp.edu.ar. Also, Department of Mathematics, Purdue University, 150 N. University Street, West Lafayette, Indiana, 47907-2067, USA*

Keywords: Seismic Attenuation, Finite Elements, Velocity Dispersion, Effective Media.

Abstract. An important upscaling effect in heterogeneous poroelastic Biot media is the dissipation mechanism due to wave-induced fluid flow caused by mesoscopic scale heterogeneities, which are larger than the pore size but much smaller than the average wavelengths of the fast waves in the seismic range of frequencies. To perform numerical simulations using Biot's equations of motion, it would be necessary to employ extremely fine meshes to properly represent these mesoscopic heterogeneities. An alternative approach to model this type of Biot medium is to determine *effective* complex moduli defining locally a viscoelastic medium having in the average the same properties than the original medium. This work presents a finite element procedure combined with a Montecarlo approach to estimate the effective phase velocity and mesoscopic attenuation in highly heterogeneous porous rocks. The method involves the use of stochastic fractals to generate different stochastic parameter patterns within the porous sample. For each realization of the stochastic parameters, a local boundary value problem is solved on a representative volume of bulk material. Numerical experiments showing the implementation of the procedure are presented.

1 INTRODUCTION

One important cause of attenuation at seismic frequencies in fluid-saturated porous media is the mesoscopic loss mechanism, caused by heterogeneities in the rock and fluid properties which are small compared with the wavelengths of the fast compressional and shear waves but larger than the average pore size. These heterogeneities can be due to local variations in lithological properties or to patches of immiscible fluids. For example, a fast compressional wave traveling across a porous rock saturated with water and patches of gas induces a greater fluid pressure in the gas patches than in the water saturated parts of the material. This in turn generates fluid flow and slow Biot waves which diffuse away from the gas-water interfaces generating significant losses in the seismic range of frequencies.

Using Biot's theory, (Biot, 1956a), (Biot, 1956b), White (White et al., 1975) developed a theory predicting that a fast P-wave traveling through thin layers alternatively saturated by either gas or water can suffer strong attenuation. Numerical simulations confirming this prediction was presented in (Rubino, J. G. et al., 2007) using finite element methods to solve Biot's equations of motion in the seismic range of frequencies. Also, numerical simulations to analyze attenuation effects in an homogeneous sandstone saturated with brine and spherical gas pockets at laboratory frequencies were presented in (Carcione et al., 2003) and (Helle et al., 2003).

The main disadvantage of using numerical simulations to represent these attenuation mechanisms is that extremely fine meshes are needed to represent the mesoscopic scale heterogeneities.

An alternative approach to model these type of Biot media is to determine *effective* complex P-wave and shear moduli defining locally a viscoelastic medium having in the average the same properties than the original Biot medium.

In this work the complex P-wave and shear moduli in heterogeneous fluid-saturated porous media are obtained using *gedanken* experiments in a Montecarlo fashion. The experiments are defined as local boundary value problems on a reference representative volume of bulk material containing stochastic heterogeneities characterized by their statistical properties.

These boundary value problems represent compressibility and shear tests needed to determine these moduli for a given realization. The moments of the phase velocities and quality factors associated with these moduli were obtained by averaging over realizations of the stochastic parameters. The Montecarlo realizations were stopped when the variance of the computed quantities stabilized at a constant value.

The approximate solution of the local boundary value problems was obtained using a finite element procedure, employing standard bilinear finite element spaces for the solid phase and the vector part of the Raviart-Thomas-Nedelec mixed finite element space of order zero for the fluid phase (Raviart and Thomas, 1975; Nedelec, 1980). The procedure was validated by reproducing known solutions in the case of periodic layered media.

Numerical experiments showing the implementation of the procedure to estimate the average and variance of the phase velocities and inverse of the quality factors associated with the P-wave and shear moduli in fluid-saturated porous sandstones are presented.

2 REVIEW OF BIOT THEORY

Consider a porous solid saturated by a single phase, compressible viscous fluid and assume that the whole aggregate is isotropic. Let $u^s = (u_i^s)$ and $\tilde{u}^f = (\tilde{u}_i^f)$, $i = 1, \cdots, d$ denote the averaged displacement vectors of the solid and fluid phases, respectively, where d denotes the

Euclidean dimension. Also let

$$u^f = \phi(\tilde{u}^f - u^s), \quad \xi = -\nabla \cdot u^f,$$

where ϕ denotes the effective porosity and set $u = (u^s, u^f)$.

Let $\varepsilon_{ij}(u^s)$ be the strain tensor of the solid. Also, let $\sigma_{ij}(u)$, $i, j = 1, \cdots, d$, and $p_f(u)$ denote the stress tensor of the bulk material and the fluid pressure, respectively. Following (Biot, 1962), the stress-strain relations can be written in the form:

$$\sigma_{ij}(u) = 2\mu\, \varepsilon_{ij}(u^s) + \delta_{ij}(\lambda_c\, \nabla \cdot u^s - \alpha\, K_{av}\, \xi), \tag{1a}$$

$$p_f(u) = -\alpha\, K_{av}\, \nabla \cdot u^s + K_{av}\xi. \tag{1b}$$

The coefficient μ is equal to the shear modulus of the bulk material, considered to be equal to the shear modulus of the dry matrix. Also,

$$\lambda_c = K_c - \frac{2}{d}\mu,$$

with K_c being the bulk modulus of the saturated material. Following (Rubino, J. G. et al., 2007; Gassmann, 1951) the coefficients in (1) can be obtained from the relations

$$\alpha = 1 - \frac{K_m}{K_s}, \quad K_{av} = \left(\frac{\alpha - \phi}{K_s} + \frac{\phi}{K_f}\right)^{-1} \quad K_c = K_m + \alpha^2 K_{av},$$

where K_s, K_m and K_f denote the bulk modulus of the solid grains composing the solid matrix, the dry matrix and the saturant fluid, respectively.

Let ρ_s and ρ_f denote the mass densities of the solid grains and the fluid and let

$$\rho_b = (1 - \phi)\rho_s + \phi\rho_f$$

denote the mass density of the bulk material. Let the positive definite matrix $\mathcal{P}$ and the nonnegative matrix $\mathcal{B}$ be defined by

$$\mathcal{P} = \begin{pmatrix} \rho_b I & \rho_f I \\ \rho_f I & gI \end{pmatrix}, \quad \mathcal{B} = \begin{pmatrix} 0I & 0I \\ 0I & bI \end{pmatrix}.$$

Here I denotes the identity matrix in $R^{d\times d}$. The mass coupling coefficient g represents the inertial effects associated with dynamic interactions between the solid and fluid phases, while the coefficient b includes the viscous coupling effects between such phases. They are given by the relations

$$b = \frac{\eta}{k}, \qquad g = \frac{S\rho_f}{\phi}, \qquad S = \frac{1}{2}\left(1 + \frac{1}{\phi}\right), \tag{2}$$

where η is the fluid viscosity and k the absolute permeability. S is known as the structure or tortuosity factor.

Next, let $\mathcal{L}(u)$ be the second order differential operator defined by

$$\mathcal{L}(u) = \left(\nabla \cdot \sigma(u), -\nabla p_f(u)\right)^t.$$

Then if $\omega = 2\pi f$ is the angular frequency, in the absence of body forces, the equations of motion can be written in the form (Biot, 1956a,b):

$$-\omega^2 \mathcal{P} u(x,\omega) + i\omega \mathcal{B} u(x,\omega) - \mathcal{L}(u(x,\omega)) = 0. \tag{3}$$

It was shown in (Biot, 1956a,b) that in this type of media two compressional waves, denoted here as P1 and P2, and one shear or S wave can propagate. The P1 and S waves correspond to the classical compressional and shear waves propagating in elastic or viscoelastic isotropic solids. The additional P2 slow mode is a wave strongly attenuated in the low frequency range, associated with the motion out of phase of the solid and fluid phases.

3 THE COMPRESSIBILITY AND SHEAR EXPERIMENTS

Field measurements show that permeability values in reservoir rocks have a high degree of spatial variability and exhibit long range correlations. It is also the case that in hydrocarbon reservoirs, regions of non-uniform patchy saturation occur at gas-oil and gas-water contacts. These type of heterogeneities can be represented using stochastic fractals.

These are two examples of highly heterogeneous saturated porous media where the sizes of the heterogeneities are small as compared with the wavelengths of the fast compressional and shear waves in the seismic range of frequencies. Consequently, solving Biot's equations of motion in these type of media can be computationally very expensive or even not feasible due to the extremely fine meshes that would be needed to define the local (mesoscopic scale) heterogeneities.

The objective of this work is to define an upscaling numerical procedure to determine in a statistical framework the complex plane wave and shear moduli associated with a representative sample of our heterogeneous material. This procedure will allow in turn to define an *equivalent* viscoelastic solid where its complex moduli carry over to the macroscale the effects due to the mesoscopic scale heterogeneities.

For that purpose, the space-frequency formulation of Biot's equations of motion combined with a Montecarlo approach is particularly convenient, since it can handle complex geometries and deal with extremely large variability in stochastic parameters. The proposed algorithm is described as follows.

Equation (3) will be solved in the 2D case on a reference square $\Omega = (0, L)^2$ with boundary Γ in the (x, y)-plane containing a representative set of stochastic heterogeneities with a given distribution and size. Thus, in a Montecarlo fashion (3) will be solved for a finite number of frequencies in the seismic range and for a large number of realizations of the stochastic parameters, with boundary conditions representing compressibility and shear experiments that after averaging over realizations will yield the moments (average and variance in this case) of the phase velocities and inverse of quality factors of our heterogeneous material. To stop the Montecarlo procedure, a criteria based on the stabilization of the variance of those quantities was employed.

Set $\Gamma = \Gamma^L \cup \Gamma^B \cup \Gamma^R \cup \Gamma^T$, where

$$\Gamma^L = \{(x,y) \in \Gamma : x = 0\}, \quad \Gamma^R = \{(x,y) \in \Gamma : x = L\},$$
$$\Gamma^B = \{(x,y) \in \Gamma : y = 0\}, \quad \Gamma^T = \{(x,y) \in \Gamma : y = L\}.$$

Denote by ν the unit outer normal on Γ and let χ be a unit tangent on Γ so that $\{\nu, \chi\}$ is an orthonormal system on Γ.

For obtaining the *undrained* complex plane wave modulus of our fluid-saturated porous medium, let us consider the solution of (3) with the following boundary conditions

$$\sigma(u)\nu \cdot \nu = -\Delta p, \quad (x,y) \in \Gamma^T, \tag{4}$$
$$\sigma(u)\nu \cdot \chi = 0, \quad (x,y) \in \Gamma^T, \tag{5}$$
$$\sigma(u)\nu \cdot \chi = 0, \quad (x,y) \in \Gamma^L \cup \Gamma^R, \tag{6}$$
$$u^s \cdot \nu = 0, \quad (x,y) \in \Gamma^L \cup \Gamma^R, \tag{7}$$
$$u^s = 0, \quad (x,y) \in \Gamma^B, \tag{8}$$
$$u^f \cdot \nu = 0, \quad (x,y) \in \Gamma. \tag{9}$$

For this set of boundary conditions the solid is not allowed to move on the bottom boundary Γ^B, the fluid is not allowed to flow out of the sample, a uniform compression is applied on the boundary Γ^T and no tangential external forces are applied on the boundaries $\Gamma^L \cup \Gamma^R \cup \Gamma^T$. In the case of periodic layered media, this experiment mimics exactly the one described by White et al. (1975) for a periodic sample obtained by a mirror reflection with respect to the x-axis of the domain Ω, enclosing the periodic sample in a thin impermeable jacket and applying a uniform compression on the boundary Γ^T and its corresponding image boundary after the indicated reflection.

The *effective undrained* complex plane wave modulus $M_c(\omega)$ is recovered by measuring the vertical displacement $u_y^s(x,L)$ on the boundary Γ^T and using this value to compute the volume change associated with this compressibility experiment. The corresponding complex compressional velocity is $V_{pc}(\omega) = \sqrt{\frac{M_c(\omega)}{\rho_b}}$. The following relations allow us to estimate the effective compressional phase velocity $V_p(\omega)$ and quality factor $Q_p(\omega)$ in the form:

$$V_p(\omega) = \left[\mathrm{Re}\left(\frac{1}{V_{pc}(\omega)}\right)\right]^{-1} \qquad \frac{1}{Q_p(\omega)} = \frac{\mathrm{Im}(V_{pc}(\omega)^2)}{\mathrm{Re}(V_{pc}(\omega)^2)} \tag{10}$$

For obtaining the *effective* complex shear modulus of our fluid-saturated porous medium, let us consider the solution of (3) with the following boundary conditions

$$-\sigma(u)\nu = g, \quad (x,y) \in \Gamma^T \cup \Gamma^L \top \Gamma^R, \tag{11}$$
$$u^s = 0, \quad (x,y) \in \Gamma^B, \tag{12}$$
$$u^f \cdot \nu = 0, \quad (x,y) \in \Gamma, \tag{13}$$

where

$$g = \begin{cases} (0, \Delta p), & (x,y) \in \Gamma^L, \\ (0, -\Delta p), & (x,y) \in \Gamma^R, \\ (-\Delta p, 0), & (x,y) \in \Gamma^T. \end{cases}$$

The effective complex shear modulus $\mu(\omega)$ is recovered by measuring the horizontal displacement $u_x^s(x,L)$ at the top boundary Γ^T; the complex shear velocity is $V_{sc}(\omega) = \sqrt{\frac{\mu(\omega)}{\rho_b}}$. The corresponding shear phase velocity and quality factor are obtained as in (10).

It can be shown that for ω small uniqueness holds for the two boundary value problems defined above. The proof will appear elsewhere.

4 A VARIATIONAL FORMULATION

In order to state a variational formulation for (3) and either (4)-(9) or (11)-(13) we need to introduce some notation. For $X \subset \mathbb{R}^d$ with boundary ∂X, let $(\cdot,\cdot)_X$ and $\langle\cdot,\cdot\rangle_{\partial X}$ denote the complex $L^2(X)$ and $L^2(\partial X)$ inner products for scalar, vector, or matrix valued functions. Also, for $s \in \mathbb{R}$, $\|\cdot\|_{s,X}$ and $|\cdot|_{s,X}$ will denote the usual norm and seminorm for the Sobolev space $H^s(X)$. In addition, if $X = \Omega$ or $X = \Gamma$, the subscript X may be omitted such that $(\cdot,\cdot) = (\cdot,\cdot)_\Omega$ or $\langle\cdot,\cdot\rangle = \langle\cdot,\cdot\rangle_\Gamma$. Also, let us introduce the spaces

$$H^{1,P}_{0,B}(\Omega) = \{v \in (H^1(\Omega))^2 : v\cdot\nu = 0, \text{ on } \Gamma^L \cup \Gamma^R, v = 0 \text{ on } \Gamma^B\},$$

$$H^{1,T}_{0,B}(\Omega) = \{v \in (H^1(\Omega))^2 : v = 0 \text{ on } \Gamma^B\},$$

$$H_0(\mathrm{div};\Omega) = \{v \in [L^2(\Omega)]^2 : \nabla\cdot v \in L^2(\Omega), v\cdot\nu = 0, \text{ on } \Gamma\}.$$

The spaces $H^{1,P}_{0,B}$ and $H^{1,T}_{0,B}$ are closed subspaces of $H^1(\Omega)$. Also, the norm in $H_0(\mathrm{div};\Omega)$ is given by

$$\|v\|_{H(\mathrm{div};\Omega)} = \left[\|v\|_0^2 + \|\nabla\cdot v\|_0^2\right]^{1/2}.$$

Let us introduce the spaces

$$\mathcal{V}^{(P)} = \left[H^{1,P}_{0,B}(\Omega)\right]^2 \times H_0(\mathrm{div};\Omega), \quad \mathcal{V}^{(T)} = \left[H^{1,T}_{0,B}(\Omega)\right]^2 \times H_0(\mathrm{div};\Omega).$$

Then multiply equation (3) by $v = \left(v^s, v^f\right)^t \in \mathcal{V}^{(P)}$, use integration by parts and apply the boundary conditions (5), (6) and (9) to see that the solution $u^{(P)} = (u^{(s,P)}, u^{(f,P)}) \in \mathcal{V}^{(P)}$ of (3) and (4)-(9) satisfies *the weak form*:

$$\Lambda(u^{(P)}, v) = \langle \Delta p, v^s\cdot\nu\rangle_{\Gamma^T}, \qquad \forall v = \left(v^s, v^f\right)^t \in \mathcal{V}^{(P)}, \tag{14}$$

where for $u = (u^s, u^f), v = (v^s, v^f) \in [H^1(\Omega)]^2 \times H(\mathrm{div};\Omega)$, the bilinear form $\Lambda(u,v)$ is defined by

$$\Lambda(u,v) = -\omega^2(\mathcal{P}u, v) + i\omega(\mathcal{B}u, v) + \sum_{l,m}(\tau_{lm}(u), \varepsilon_{lm}(v^s)) - \left(p_f(u), \nabla\cdot v^f\right).$$

Similarly, the solution $u^{(T)} = (u^{(s,T)}, u^{(f,T)}) \in \mathcal{V}^{(T)}$ of (3) and (11)-(13) satisfies *the weak form*:

$$\Lambda(u^{(T)}, v) = \langle g, v^s\rangle_{\Gamma^T}, \qquad \forall v = \left(v^s, v^f\right)^t \in \mathcal{V}^{(S)}. \tag{15}$$

Uniqueness of the solution of the boundary value problem (3) and either (4)-(9) or (11)-(13) and its variational formulations (14) or (15) can be demonstrated for ω sufficiently small using Poincare's inequality. Existence will be assumed.

5 THE FINITE ELEMENT PROCEDURES

Let $\mathcal{T}^h(\Omega)$ be a non-overlapping partition of Ω into rectangles Ω_j of diameter bounded by h such that $\overline{\Omega} = \cup_{j=1}^J \overline{\Omega}_j$. Different finite element spaces, denoted $\mathcal{N}^{h,P}_{0,B} \subset H^{1,P}_{0,B}(\Omega)$ and $\mathcal{N}^{h,T}_{0,B} \subset H^{1,T}_{0,B}(\Omega)$ will be used to approximate the solid displacement vector for the compressibility and shear tests models, respectively. They are defined as follows

$$\mathcal{N}^{h,P}_{0,B} = \{v : v|_{\Omega_j} \in P_{1,1}\times P_{1,1}, v\cdot\nu = 0, \text{ on } \Gamma^L\cup\Gamma^R, v = 0 \text{ on } \Gamma^B\} \cap [C^0(\overline{\Omega})]^2$$
$$\mathcal{N}^{h,T}_{0,B} = \{v : v|_{\Omega_j} \in P_{1,1}\times P_{1,1}, v = 0 \text{ on } \Gamma^B\} \cap [C^0(\overline{\Omega})]^2,$$

where $P_{1,1}$ denotes the polynomials of degree not greater than 1 on each variable.

To approximate the fluid displacement a closed subspace of the vector part of the Raviart-Thomas-Nedelec space of zero order, denoted $\mathcal{W}_0^h$, was employed (Raviart and Thomas, 1975), (Nedelec, 1980). It is defined as

$$\mathcal{W}_0^h = \{v : v|_{\Omega_j} \in P_{1,0} \times P_{0,1},\ v \cdot \nu = 0,\ \text{on } \Gamma\}.$$

Let

$$\Pi_h^{(P)} : \left[H^2(\Omega) \cap H_{0,B}^{1,P}(\Omega)\right]^2 \to \mathcal{N}_{0,B}^{h,P}, \quad \Pi_h^{(T)} : \left[H^2(\Omega) \cap H_{0,B}^{1,T}(\Omega)\right]^2 \to \mathcal{N}_{0,B}^{h,T}$$

be the projections defined locally such that $\Pi_h^{(P)}|_{\Omega_j} = \Pi_{h,j}^{(P)},\ \Pi_h^{(T)}|\Omega_j = \Pi_{h,j}^{(T)}$, where

$$\begin{aligned}
&(\Pi_{h,j}^{(P)}\varphi - \varphi, v) = 0, \quad v \in P_{1,1} \times P_{1,1},\ v \cdot \nu = 0,\ \text{on } \Gamma^L \cup \Gamma^R, v = 0 \text{ on } \Gamma^B,\\
&(\Pi_{h,j}^{(T)}\varphi - \varphi, v) = 0, \quad v \in P_{1,1} \times P_{1,1},\ v = 0 \text{ on } \Gamma^B.
\end{aligned}$$

Also, let

$$Q^h : H_0^1(\mathrm{div};\Omega) \to \mathcal{W}_0^h$$

be the projection defined by

$$\langle (Q_h\psi - \psi) \cdot \nu, 1\rangle_B = 0, \quad B = \partial\Omega_j \cap \partial\Omega_k \text{ or } B = \partial\Omega_j \cap \partial\Omega.$$

It is well known that, for all $\varphi \in [H^2(\Omega) \cap H_{0,B}^{1,P}(\Omega)]^2$, $\psi \in [H^2(\Omega) \cap H_{0,B}^{1,T}(\Omega)]^2$ and $\eta \in H_0^1(\mathrm{div};\Omega)$ (Ciarlet, 1980; Nedelec, 1980; Raviart and Thomas, 1975)

$$\|\varphi - \Pi_h^{(P)}\varphi\|_0 + h\|\varphi - \Pi_h^{(P)}\varphi\|_1 \le Ch^2\|\varphi\|_2, \tag{16a}$$
$$\|\psi - \Pi_h^{(T)}\psi\|_0 + h\|\psi - \Pi_h^{(T)}\psi\|_1 \le Ch^2\|\psi\|_2, \tag{16b}$$
$$\|\eta - Q^h\eta\|_0 \le Ch\|\eta\|_1, \tag{16c}$$
$$\|\eta - Q^h\eta\|_{H(\mathrm{div};\Omega)} \le Ch\left(\|\eta\|_1 + \|\nabla \cdot \eta\|_1\right). \tag{16d}$$

Let us define the finite element spaces

$$\mathcal{V}^{(h,P)} = \mathcal{N}_{0,B}^{h,P} \times \mathcal{W}^h, \quad \mathcal{V}^{(h,T)} = \mathcal{N}_{0,B}^{h,T} \times \mathcal{W}^h.$$

Then the finite element procedure to compute the approximate solution of the compression problem (14) is defined as follows: find $u^{(h,P)} = \left(u^{(s,h,P)}, u^{(f,h,P)}\right)^t \in \mathcal{V}^{h,P}$ such that

$$\Lambda(u^{(h,P)}, v) = \langle \Delta p, v^s \cdot \nu\rangle_{\Gamma^T}, \qquad v = \left(v^s, v^f\right)^t \in \mathcal{V}^{(h,P)}. \tag{17}$$

Similarly, the finite element procedure to compute the approximate solution of the shear problem (15) is: find $u^{(h,T)} = \left(u^{(s,h,T)}, u^{(f,h,T)}\right)^t \in \mathcal{V}^{(h,T)}$ such that

$$\Lambda(u^{(h,T)}, v) = \langle g, v^s\rangle_{\Gamma^T}, \qquad v = \left(v^s, v^f\right)^t \in \mathcal{V}^{(h,T)}. \tag{18}$$

Since $u^{(h,P)} \in H_{0,B}^{1,P}, u^{(h,T)} \in H_{0,B}^{1,T}$, uniqueness for the discrete problems (17) and (18) follows with the same argument than for the continuous case provided the frequency ω is small. Existence follows from finite dimensionality.

The following *a priori* error estimates can be derived.

Theorem 5.1 *For ω small, the solutions $u^{(h,P)}, u^{(h,T)}$ of problems* (17) *and* (18) *satisfy the following a priori error estimates*

$$\begin{aligned} &\|u^{(s,h,P)} - u^{(s,P)}\|_1 + \|u^{(f,h,P)} - u^{(f,P)}\|_0 + \|\nabla \cdot \left(u^{(f,h,P)} - u^{(s,P)}\right)\|_0 \\ &\qquad \leq C_{11}(\omega) h \left(\|u^{(s,P)}\|_2 + \|u^{(f,P)}\|_1 + \|\nabla \cdot u^{(f,P)}\|_1\right), \end{aligned} \tag{19}$$

$$\begin{aligned} &\|u^{(s,h,T)} - u^{(s,T)}\|_1 + \|u^{(f,h,T)} - u^{(f,T)}\|_0 + \|\nabla \cdot \left(u^{(f,h,T)} - u^{(s,T)}\right)\|_0 \\ &\qquad \leq C_{11}(\omega) h \left(\|u^{(s,T)}\|_2 + \|u^{(f,T)}\|_1 + \|\nabla \cdot u^{(f,T)}\|_1\right). \end{aligned} \tag{20}$$

6 A MONTECARLO APPROACH FOR STOCHASTIC FRACTAL PARAMETER DISTRIBUTIONS

For the compressibility test, let us consider a porous sample with a spatially variable gas - water distribution in the form of irregular *patches* fully saturated with gas and zones fully saturated with water. No mixing nor capillary forces are taken into account and the two fluids are assumed to occupy different mesoscopic regions of the model.

The generation of these kind of heterogeneities involves the use of a stochastic fractal field, based on the so-called von Karman self-similar correlation functions. These models are widely used in the statistical characterization of heterogeneities for different applications.

Following (Frankel and Clayton, 1986) and more recently (Santos, J. E. et al., 2005), we consider a particular case for which the spectral density of the stochastic field is given by:

$$S_d(q_x, q_y) = S_0(1 + q^2 a^2)^{-(H+E/2)} \tag{21}$$

where $q = \sqrt{q_x^2 + q_y^2}$ is the radial wavenumber, a the correlation length, H is a self-similarity coefficient ($0 < H < 1$), S_0 is a normalization constant and E is the Euclidean dimension. Equation (21) corresponds to a fractal process of dimension $D = E + 1 - H$ at scales smaller than a.

The first step to generate a patchy fluid distribution is to assign to each subdomain Ω_j of the partition $\mathcal{T}^h$ a pseudo-random number using a generator with uniform distribution associated with a given *seed* number giving a realization n. This random field is Fourier transformed to the spatial wavenumber domain and its amplitude spectrum is filtered using equation (21). The result is then transformed back to the spatial domain, obtaining a *micro-heterogeneous* gas saturation model $S_g^{(j)}, j = 1, \cdots, J$. Next, to construct the patchy distribution, i.e. the *mesoscopic* heterogeneities, we established different water saturation threshold values S_w^* so that for each subdomain Ω_j where $S_g^{(j)} \leq S_w^*$ we changed the value to 100% gas saturation (i.e. 0% water saturation) and for $S_g^{(m)} > S_w^*$ we consider 0% gas saturation. In this way for a given realization and a fixed value of S_w^*, an overall gas saturation $\bar{S}_g$ is obtained for the computational rock sample.

For a given realization n of patchy distribution with associated overall gas saturation $\bar{S}_g$, the numerical problem (3) with boundary conditions (4) - (9) was solved for a finite number of frequencies $\omega_m, m = 1, \cdots, N_F$ in the seismic range, from where the values of $V_p^n(\omega_m)$ and $1/Q_p^n(\omega_m)$ are obtained.

This procedure was repeated for a large number of realizations $n = 1, \cdots, N_R$, and the statistical behavior of $V_p^n(\omega_m)$ and $1/Q_p^n(\omega_m)$ after N_R realizations was analyzed by computing

the mean and variance of these quantities in the form:

$$\langle V_p(\omega_m, N_R)\rangle = \frac{1}{N_R}\sum_{n=1}^{N_R} V_p^n(\omega_m), \tag{22}$$

$$\sigma^2_{V_p}(\omega_m, N_R) = \frac{1}{(N_R-1)}\sum_{n=1}^{N_R}\left[V_p^n(\omega_m) - \langle V_p(\omega_m, N_R)\rangle\right]^2. \tag{23}$$

The corresponding standard deviation is $\sqrt{\sigma^2_{V_p}(\omega_m, N_R)}$. Analogous definitions were used to obtain the statistics associated with the inverse of the quality factor $Q_p(\omega)$.

For the shear test, we choose to perform the numerical experiments on a porous sample with heterogeneities in the petrophysical properties and an uniform water distribution. The heterogeneous porous matrix is composed of two materials with fractal distribution, a sandstone and a shaley sandstone. Even for the case of pure shear, the presence of this type of heterogeneities can produce fluid pressure gradients causing mesoscopic loss effects.

To analyze the convergence of the Montecarlo approach in terms of the number of realizations N_R, the frequency average of the variances was computed by

$$\| \sigma_l^2(N_R) \| = \left[\frac{1}{N_F}\sum_{m=1}^{N_F}\sigma_l^2(\omega_m, N_R)\right]^{1/2}, \quad l = V_p, V_s, Q_p, Q_s. \tag{24}$$

The Montecarlo simulations were stopped when the variance (24) of the computed quantities stabilized at a constant value.

7 NUMERICAL EXPERIMENTS

The finite element procedures (17) and (18) were implemented to obtain the (effective) complex frequency dependent plane wave and shear moduli for sandstones saturated with an irregular *patchy* distribution of gas and water. For the compressibility tests, the following material properties (taken from Carcione J.M. and Picotti S. (2006)) were used: absolute porosity $\phi = 0.3$, matrix permeability $\kappa = 10^{-12}$ m^2, mineral bulk modulus $K_s = 37$ GPa, dry matrix bulk modulus $K_m = 4.8$ GPa and shear moduli $\mu = 4.8$ GPa, water bulk modulus $K_w = 2.25$ GPa, water viscosity $\eta_w = 0.03$ Poise, gas bulk modulus $K_g = 0.012$ GPa and gas viscosity $\eta_g = 0.0015$ Poise.

First, to validate the code, Figure 1 displays the results of the compressibility model to obtain the P-wave phase velocities and inverse of quality factors for the case in which the sample is a periodic medium consisting of alternating layers of equal thickness 40 cm saturated with either gas or water (i.e. $\bar{S}_g = 0.5$). As can be observed in Figures 1a and 1b, the computed values are in excellent agreement with those predicted by White's theory (White et al., 1975).

To validate the code for the case of the shear test, it was checked that for uniform either gas or water saturation, the code yields the *real* shear modulus at the zero limit frequency.

The next set of experiments shows the results of the Montecarlo procedure for the compressibility tests in the case of patchy saturation. The computational domain Ω was chosen to be a square of size $L = 70$ cm with a uniform partition $\mathcal{T}^h$ of Ω into squares Ω_j of side length $h = L/75$. The parameters needed in (21) to generate the patchy gas-water distributions were $E = 2, a = 10$cm$, D = 2.2$. For each realization, the water threshold value S_w^* was adjusted to obtain an overall gas saturation $\bar{S}_g = 0.1$. The excitation frequency was varied from 0 to

(a)

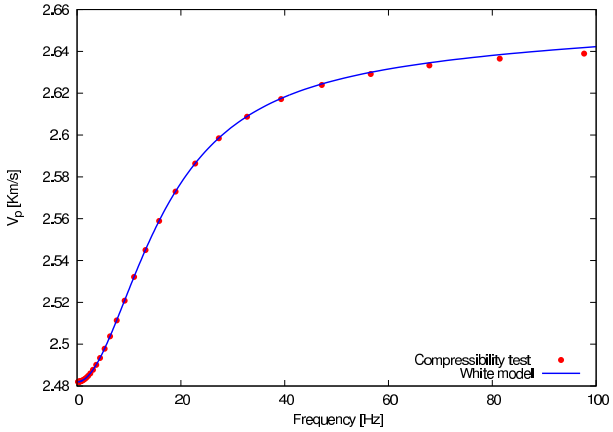

(b)

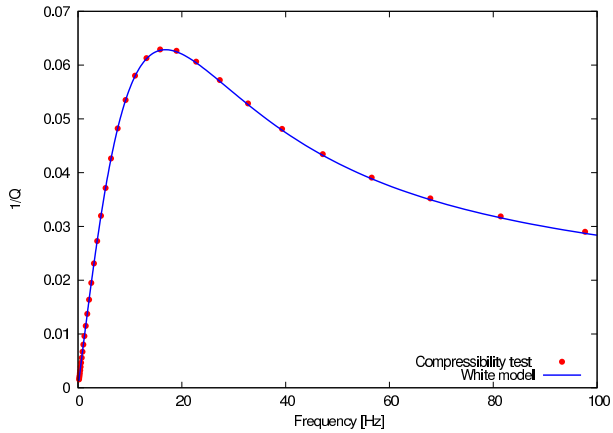

Figure 1: Comparison between the compressional velocity (a), and the inverse quality factor (b) obtained using White's model and the numerical compressibility test.

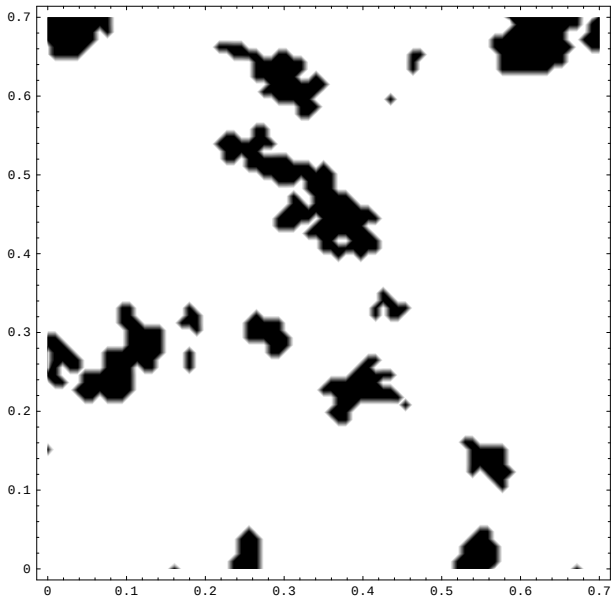

Figure 2: Example of patchy fluid distribution. The black zones correspond to 100 % gas saturation and the white zones to 100 % water saturation in the pores. Overall gas saturation $\bar{S}_g = 0.1$

60 Hz using N_F =15 equally spaced values. Other types of heterogeneities, such as fractal porosity-permeability distributions may be analyzed (Santos, J. E. et al., 2005), but they are not considered here for brevity.

Once the solution $u^{(h,P)}$ of (14) is obtained, the *undrained* complex plane wave modulus $M_c(\omega)$ is easily obtained as indicated in Section 3, and the corresponding phase velocities and quality factors are obtained as in (10).

Figure 2 illustrate a realization of the patchy gas-water distribution, where the black zones correspond to 100 % gas saturation and the white zones to 100 % water saturation in the pores. Figure 3 shows the mean compressional velocity versus frequency after 70 realizations and the corresponding standard deviations (which are indicated using dotted lines), where the important velocity dispersion with frequency within the seismic range can be observed.

Next in Figure 4 we illustrate the behavior of the mean inverse compresional quality factor versus frequency (after the 70 realizations) and their corresponding standard deviations, indicated again using dotted lines. Note the noticeable very low values of Q_p with a peak of $\frac{1}{Q_p}$ near 20 Hz, demonstrating clearly the mesoscopic loss mechanism. Also, in the low frequency limit we observe that the attenuation varies almost linearly with frequency.

Figures 5 and 6 display the variance of the compressional velocities and inverse quality factors averaged in the whole range of frequencies for different values of N_R (computed according to (24)). In both cases it is interesting to observe the stabilization and the low values of these statistical properties, which suggests that for a given $\bar{S}_g$ the averaged effective velocities and inverse quality factors obtained give representative values for the chosen overall saturation $\bar{S}_g$.

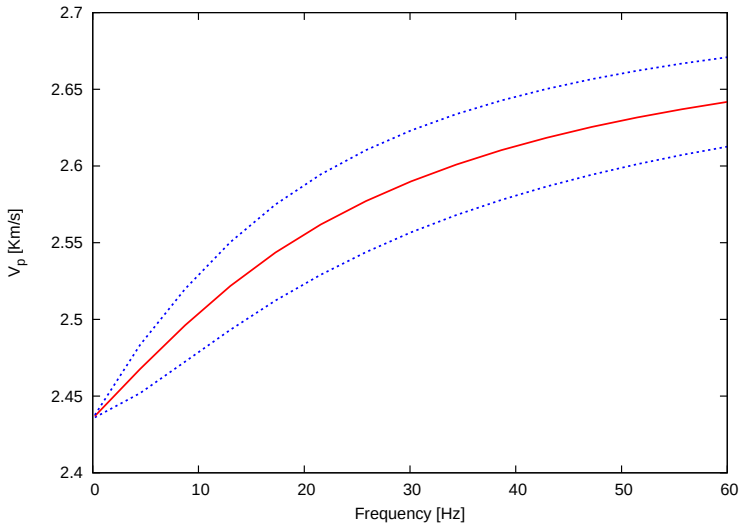

Figure 3: Mean of the compressional phase velocity vs. frequency (solid lines). Dotted lines indicate the corresponding standard deviations. Overall gas saturation $\bar{S}_g = 0.1$

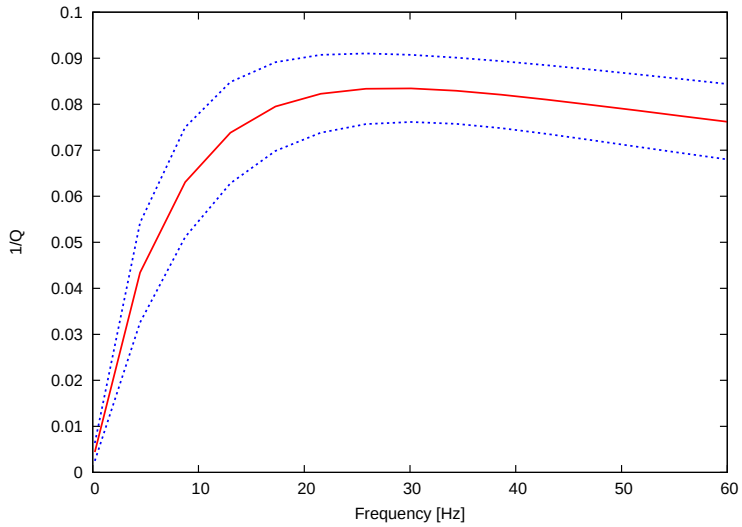

Figure 4: Mean of the compressional inverse quality factor vs. frequency (solid lines). Dotted lines indicate the corresponding standard deviations. Overall gas saturation $\bar{S}_g = 0.1$

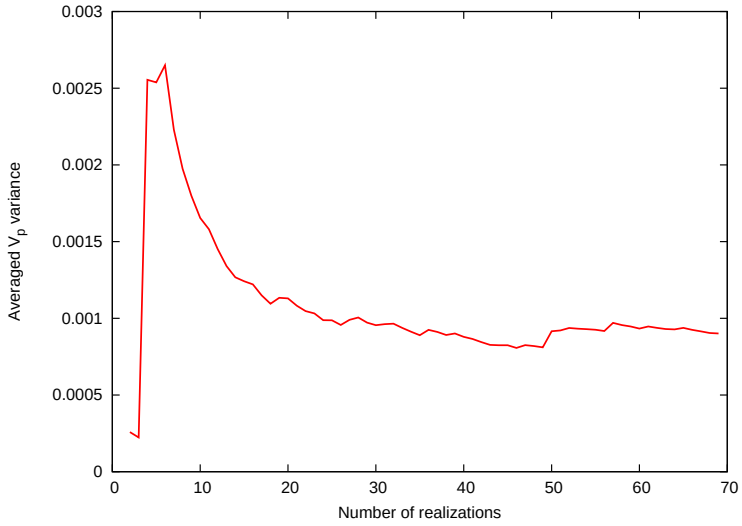

Figure 5: Averaged variance of the compressional velocity for $\bar{S}_g = 0.1$ as a function of the total number of realizations.

The same behavior is observed for the other overall saturations but for brevity they are not shown in this work. As expected, when the shear test was performed for the patchy saturation case, very small values of velocity dispersion and attenuation were obtained.

Instead, as indicated above, the shear test was applied to a water saturated heterogeneous porous matrix composed of two different materials with fractal distribution, a sandstone and a shaley sandstone, with fractal parameters $E = 2, D = 2.2, a = 30$ cm. The sandstone has porosity $\phi = 0.4$, mineral bulk modulus $K_s = 39$ GPa, dry matrix bulk modulus $K_m = 3.9$ GPa and shear moduli $\mu = 3.9$ GPa, while the shaley sandstone, of porosity $\phi = 0.2$, has mineral bulk modulus $K_s = 34.25$ GPa, dry matrix bulk modulus $K_m = 16.1$ GPa and shear moduli $\mu = 12.5$ GPa. These values for the properties of the two materials were obtained using the model in Goldberg, I. and Gurevich, B. (1997). The water properties were the same used above for the compressibility test. The permeability for both materials was determined using the Kozeny-Carman relation (Mavko et al., 1998) for an average grain size. The domain and mesh sizes were the same as in the compressibility test.

Figure 7 shows a realization of the heterogeneous shaley sandstone used to perform the shear test, where the black zones correspond to 100 % sandstone and the white zones to 100 % shaley sandstone. The following picture (Figure 8) displays the computed shear phase velocity versus frequency, which shows very little dispersion. The corresponding inverse of the quality factor is plotted in Figure 9, which shows a peak at approximately 15 Hz. For this example, the mesoscopic loss mechanism is less noticeable than in the case of the compressibility test and patchy fluid distribution. The corresponding statistical analysis was performed showing the stabilization of the variance as in the previous example and it is not shown here for brevity. Further research to determine higher attenuation effects for shear waves in heterogeneous porous materials is currently being performed.

8 CONCLUSIONS

In this paper a finite element procedure to estimate the effective phase velocity and mesoscopic attenuation in highly heterogeneous saturated porous rocks is presented.

The methodology is based on the finite element solution of the classical Biot equations to

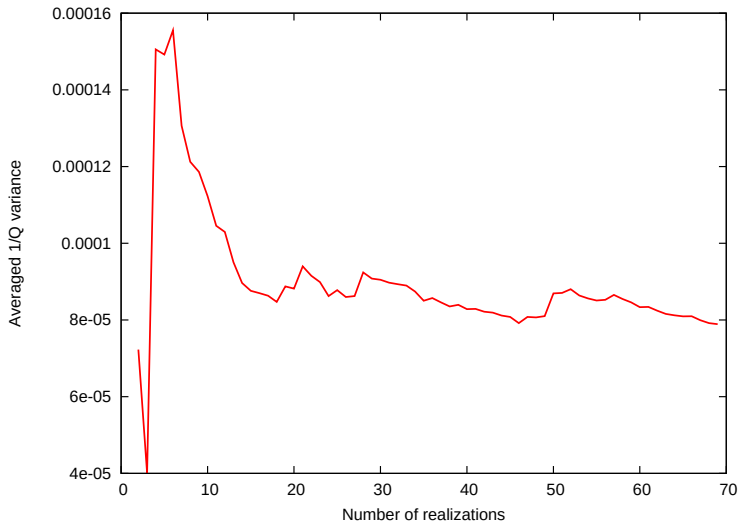

Figure 6: Averaged variance of the compressional inverse quality factor for $\bar{S}_g = 0.1$ as a function of the total number of realizations.

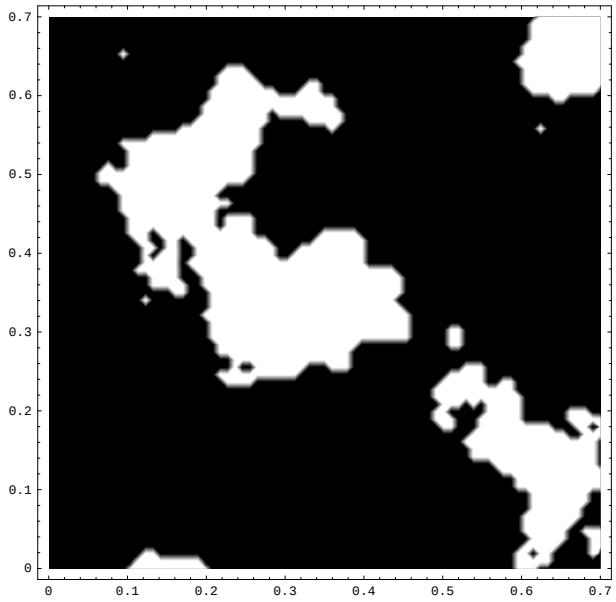

Figure 7: Example of an heterogeneous lithologic distribution. The black zones correspond to 100 % sandstone and the white zones to 100 % shaley sandstone.

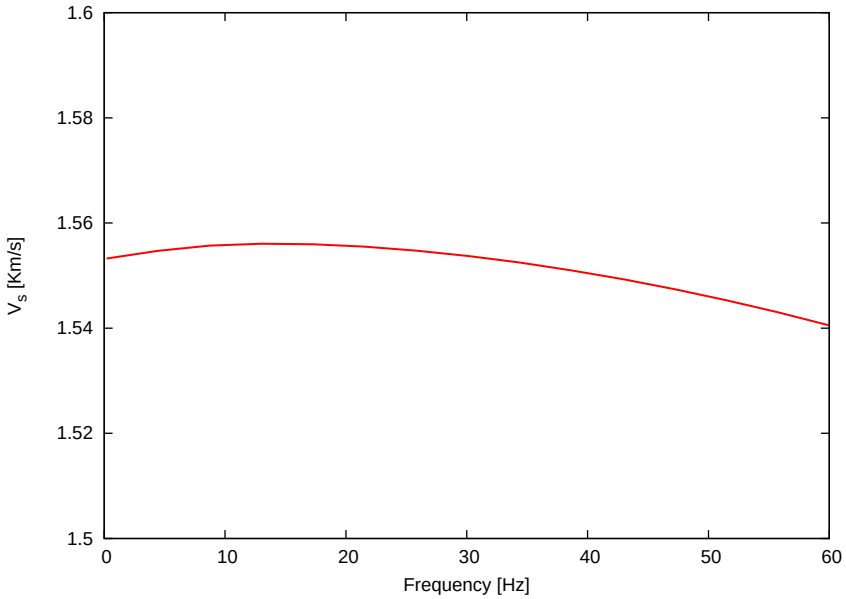

Figure 8: Shear phase velocity V_s vs. frequency.

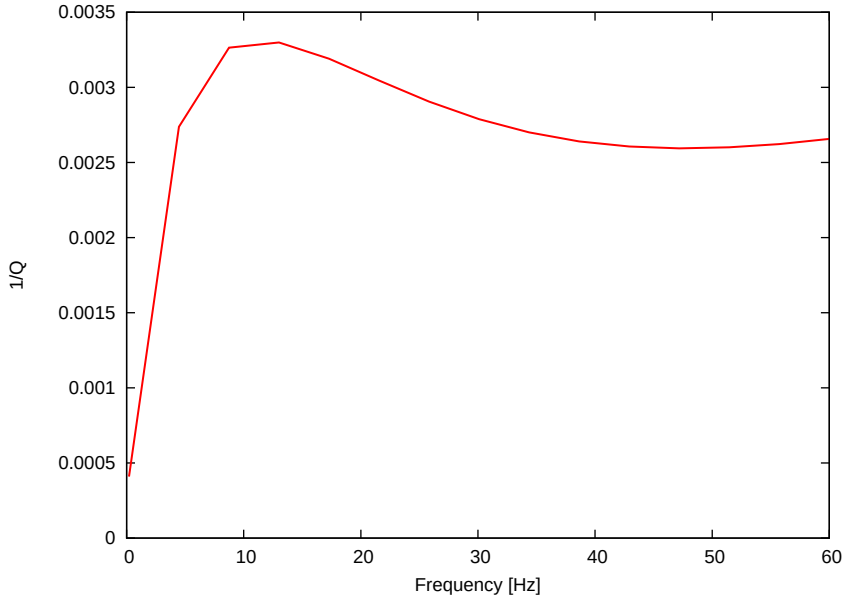

Figure 9: Inverse of the quality factor Q_s vs. frequency.

simulate oscillatory compressibility and shear tests, combined with a Montecarlo approach to obtain the complex effective plane wave and shear modulus for different heterogeneity patterns. Unlike the theoretical White's theory (White et al. (1975)) valid only for periodic layered media, our method allows to simulate any distribution of heterogeneities within the domain.

In the case of patchy saturation, our results indicate that in the frequency range analyzed, the presence of small patches of gas (i.e., low overall gas saturation values $\bar{S}_g$) cause strong dispersion and attenuation effects. In particular, the very low values of the quality factors confirm the importance of the mesoscopic loss mechanism in the presence of irregular heterogeneities, which may result in strong amplitude decays of a seismic signal traveling through a reservoir rock. Since this mechanism is negligible for the case of homogeneous fluid distributions, a careful analysis of seismic amplitudes and velocities may help to understand and discriminate the saturation type (homogeneous or heterogeneous) and the overall fluid content.

In the case of an heterogeneous porous matrix composed of two types of lithology with fractal distribution and uniform fluid saturation, the effective shear phase velocities show little dispersion and the values of the quality factors are not so significant as in the compressibility experiment. We noticed that in this type of materials the mesoscopic loss mechanism is very sensitive to the shapes and sizes of the heterogeneities.

Although the present conclusions are based on the analysis performed in the seismic frequency range, the methodology described in this work can be extended to the high frequency range (such as the sonic or ultrasonic).

9 AKNOWLEDGEMENTS

This work was partially funded by CONICET, Argentina (PIP 5126/05) and the Agencia Nacional de Promoción Científica y Tecnológica (ANPCyT), PICT 2003, #03-13376.

REFERENCES

Biot M.A. Theory of propagation of elastic waves in a fluid-saturated porous solid. I. Low frequency range. *J. Acoust. Soc. Am.*, 28:168–171, 1956a.

Biot M.A. Theory of propagation of elastic waves in a fluid-saturated porous solid. II. High frequency range. *J. Acoust. Soc. Am.*, 28:179–191, 1956b.

Biot M.A. Mechanics of deformation and acoustic propagation in porous media. *J. Appl. Phys.*, 33:1482–1498, 1962.

Carcione J.M., Helle H.B., and Pham N.H. White's model for wave propagation in partially saturated rocks: Comparison with poroelastic numerical experiments. *Geophysics*, 68:1389–1398, 2003.

Carcione J.M. and Picotti S. P-wave seismic attenuation by slow-wave diffusion: Effects of inhomogeneous rock properties. *Geophysics*, 71:O1–O8, 2006.

Ciarlet P.G. *The Finite Element Method for Elliptic Problems*. Noth Holland, 1980.

Frankel A. and Clayton R.W. Finite difference simulation of seismic wave scattering: implications for the propagation of short period seismic waves in the crust and models of crustal heterogeneity. *J. Geophys. Res.*, 91:6465 – 6489, 1986.

Gassmann F. über die elastizität poröser medien" ("on the elasticity of porous media"). *Vierteljahrsschrift der Naturforschenden Gessellschaft in Zurich*, pages 1–23, 1951.

Goldberg, I. and Gurevich, B. A semi-empirical velocity-porosity-clay model for petrophysical interpretation of p- and s- velocities. *Geophysical Prospecting*, 46:271–285, 1997.

Helle H.B., Pham N.H., and Carcione J.M. Velocity and attenuation in partially saturated rocks.

poroelastic numerical experiments. *Geophysical Prospecting*, 51:551–566, 2003.

Mavko G., Mukerji T., and Dvorkin J. The rock physics handbook. *Cambridge University Press*, 1998.

Nedelec J.C. Mixed finite elements in r^3. *Numer. Math.*, 35:315–341, 1980.

Raviart P.A. and Thomas J.M. Mixed finite element method for 2^{nd} order elliptic problems. *Mathematical Aspects of the Finite Element Methods, Lecture Notes of Mathematics, vol. 606, Springer*, 1975.

Rubino, J. G., Santos, J. E., Picotti S., and Carcione J.M. Simulation of upscaling effects due to wave-induced fluid flow in biot media using the finite-element method. *J. Appl. Geophys. (in press)*, 2007.

Santos, J. E., Ravazzoli, C. L., Gauzellino, P. M., and Carcione, J. M. Numerical simulation of ultrasonic waves in reservoir rocks with patchy saturation and fractal petrophysical properties. *Computational Geosciences*, 9:1–27, 2005.

White J.E., Mikhaylova N.G., and Lyakhovitskiy F.M. Low-frequency seismic waves in fluid-saturated layered rocks. *Izvestija Academy of Siences USSR, Physics of Solid Earth*, 10:654–659, 1975.